International Global Navigation Satellite Systems Association
IGNSS Symposium 2020

Colombo Theatres, Kensington Campus, UNSW Australia
5 – 7 February 2020

Assessment of the New DFMC and PPP services of the second-generation SBAS in the Mining and Urban environments

Kan Wang
School of Earth and Planetary Sciences, Curtin University, Australia
Tel: +61892663157, Email: kan.wang@curtin.edu.au
Ahmed El-Mowafy
School of Earth and Planetary Sciences, Curtin University, Australia
Tel: +61892663403, Email: A.El-Mowafy@curtin.edu.au
Mehdi Khaki
School of Engineering, University of Newcastle, Australia
Tel: +61249216626, Email: Mehdi.Khaki@newcastle.edu.au
Troy Sutherland
Roy Hill, Whitham Road, Perth Airport, WA 6105, Australia
Tel: +61862421000, Email: troy.sutherland@royhill.com.au
Eldar Rubinov
FrontierSI, Data61 at Village St and Fishplate Ln, Docklands VIC 3008, Australia
Tel: +61402607290, Email: erubinov@frontiersi.com.au

ABSTRACT

In 2017, a two-year test-bed for a second generation Satellite-Based Augmentation System (SBAS) was initiated in Australia and New Zealand in preparation for building an operational system. In addition to the traditional SBAS L1 service for GPS, the test-bed provided the dual-frequency multi-constellation (DFMC) SBAS service, and the precise point positioning (PPP) service using GPS and Galileo. In this study, and for the first time, the positioning performance of the different SBAS services is presented in the mining sector. It is shown that after convergence of the horizontal PPP solutions, the RMSE is at sub-dm to dm. Furthermore, this contribution presents and compares two weighting models that can benefit the new DFMC SBAS in environments with large multipath, firstly not considering the signal smoothing time and secondly considering it. The results show that considering the smoothing time in the weighting model is helpful to improve the positioning accuracy without degrading the availability.

KEYWORDS: SBAS; DFMC; PPP; GPS; Galileo

1. INTRODUCTION

Over more than 20 years, the Satellite-Based Augmentation System (SBAS) has been developed

in different countries to augment positioning and navigation services. SBAS improves the accuracy, integrity and availability of GNSS positioning results by transmitting ranging and integrity information as well as corrections such as satellite orbits, satellite clocks and regional ionospheric corrections from geostationary (GEO) satellites. Existing SBAS services include the American Wide Area Augmentation System (WAAS), the European Geostationary Navigation Overlay Service (EGNOS), the Japanese Multi-functional Satellite Augmentation System (MSAS), the Russian System for Differential Correction and Monitoring (SDCM) and the Indian GPS-aided GEO Augmented Navigation (GAGAN) with an overview given in Choy *et al.* (2017).

The first generation SBAS transmits signals on the L1 frequency (1575.42 MHz) in accordance with the Radio Technical Commission for Astronautics (RTCA) Minimum Operational Performance Standards (MOPS), with the latest version known as RTCA DO-229E. The SBAS corrections, including also the regional ionospheric delays, need to be computed and sent to users to augment single-frequency GNSS signals. This on one side increases the sensitivity of the positioning results to the accuracy of the ionospheric delays, and on the other side limits the service area to the area covered by the Continuously Operating Reference Stations (CORS) network used for processing the SBAS ionosphere corrections. In the second generation SBAS, dual-frequency multi-constellation (DFMC) service is provided to users with the messages transmitted via the L5 frequency (1176.45 MHz). This enables the elimination of the dominant first-order term of the ionospheric delays by forming ionosphere-free linear combination using the two frequencies. The service area is thus extended to the entire GEO footprint, as only satellite-related information like satellite orbits and clocks are needed in such case (Barrios *et al.*, 2018). Transmitting the corrections on the L5 frequency has the advantage that it is shared by an increasing number of satellites from different Global Navigation Satellite Systems (GNSSs) and Regional Navigation Satellite Systems (RNSSs), now and in the future, i.e. the GPS IIF and III satellites on L5, the Galileo satellites on E5a, the future GLONASS-KM satellites on L5, Beidou satellites BDS-3 on B2a, the satellites from the Japanese Quasi-Zenith Satellite System (QZSS) on L5 and the satellites from Indian Regional Navigation Satellite System (IRNSS) on L5. The resistance of the L5 signals against the interference problem makes it suitable for safety-of-life applications, mainly aviation.

In February 2017, Australia and New Zealand commenced a two-year SBAS test-bed in both countries as a pre-step of the building process of a new system that is planned to be fully operational within a few years. Geoscience Australia (GA), Land Information New Zealand (LINZ) and FrontierSI (previously Cooperative Research Centre for Spatial Information - CRCSI) ran the test-bed in co-operation with the service providers GMV, Lockheed Martin Space Systems Company and Inmarsat (Technical Specifications 2017). The test-bed aimed at evaluating the performance of the new generation of SBAS not only in aviation, but also in major sectors such as mining, transport, agriculture, and marine services. In addition to the L1 legacy SBAS signals, the test-bed provided the DFMC SBAS corrections broadcast over the L5 frequency as well as the Precise Point Positioning (PPP) service (in ambiguity-float mode) broadcast over both L1 and L5. This service allows for PPP positioning anywhere in the footprint of the SBAS satellite, i.e., in Australia-Asia-Pacific region, whereas traditional PPP depends on receiving the corrections via the Internet, and thus is limited to areas where the Internet is available. Some studies related to the SBAS test-bed messages and positioning results have been performed in the past two years (Barrios *et al.,* 2018; Cogdell and Reddan, 2018; Sobreira *et al.*, 2018). The improved positioning accuracy of SBAS and PPP services could lead to large economic benefits in diverse sectors, as the high-precision positioning provided by the new generation of SBAS relies on single receiver and is free of charge.

In this contribution, for the first time, we present a performance analysis of different types of SBAS solutions within the SBAS test-bed for various mining applications. Experiments were carried out under harsh weather and working conditions at actual mining sites. Additionally, two weighting models are compared for applications in complicated environment with large multipath. The first model does not consider the smoothing time during carrier-phase smoothing the code observations, and the second model takes the smoothing time into consideration.

In the next section, the SBAS test-bed is briefly introduced, followed by a section explaining the processing strategies. The experiments are presented and their results are analysed in the subsequent section with discussions followed. Finally, findings are summarized and recommendations are given.

2. SBAS TEST-BED

The SBAS test-bed initiated by GA, LINZ and FrontierSI aimed to assess the SBAS performance over a diversity of industries including mining, aviation, agriculture, road, rail and maritime applications. As illustrated in Figure 1, the SBAS infrastructure consists of the space segment, the ground segment, and the support segment in addition to the user segment. The space segment consists of the GNSS satellites (in this case GPS and Galileo), and the GEO satellite Inmarsat-4F1 with a PRN of 122. It broadcasts GNSS signals and SBAS messages that are to be received by the users and processed by the ground segment. The ground segment consists of three parts. The CORS network collects raw GNSS observations streamed from different networks in real time. The data is then transferred to the Augmentation Processing Center (APC) at Uralla, NSW, which computes the precise SBAS/PPP orbit/clock corrections and the integrity information to be transmitted in the SBAS messages. The uplink system captures these messages, transforms them into electromagnetic signals and sends them to the GEO satellite. The support segment is a separate magicGNSS Web Monitor at the GMV's premises in Spain. It monitors the system and service performance in both the real-time and post-processing modes, provides information like protection levels, ionosphere conditions and the number and performances of the monitored satellites. The tool can be accessed by authorized users through a web server (Technical Specifications, 2017; Barrios *et al.*, 2018).

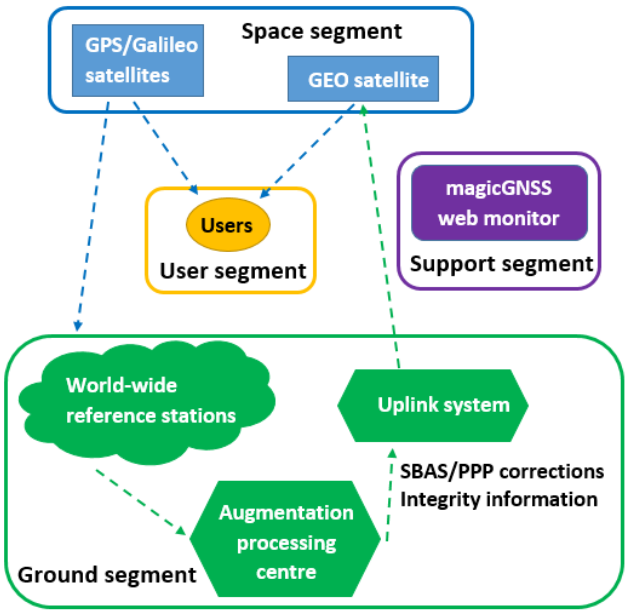

Figure 1. SBAS test-bed infrastructure

2.1 Second-generation SBAS signals

In the SBAS test-bed, different services of the second-generation SBAS are provided to target users. The SBAS L1 legacy signal is given according to RTCA/DO-229E (RTCA 2016). This legacy signal only covers the ground network area over Australia and New Zealand to transmit the regional ionospheric delays. The SBAS DFMC signal is given according to RTCM DFMC, WG62 GAL GPS SBAS MOPS v0.3.8 (Technical Specifications, 2017; *Barrios et al.*. 2018). Data from a global network with CORS from Australian Regional GNSS Network, LINZ PositioNZ network, South Pacific Regional GNSS Network (SPRGN) and the International GNSS Service (IGS) (Dow *et al.*, 2009, Noll *et al.*, 2009) real-time network were used for computing the satellite orbits and clocks. As ionosphere-free combination is formed by the dual-frequency users, the service area covers the entire footprint of the GEO Inmarsat-4F1 satellite, including the Australia-Asia-Pacific region. The PPP corrections, including the satellite orbit and clock corrections to the broadcast ephemeris (El-Mowafy *et al.*, 2017), are broadcast over the L1 and L5 SBAS signals. PPP over L1 only contains GPS corrections, whilst PPP over L5 contains GPS and Galileo corrections. The service area of the PPP service also covers the entire footprint of Inmarsat-4F1. As only the GPS IIF satellites are transmitting GPS signals on L5 and the number of the operational GPS IIF satellites are still limited (currently 12 in August 2019), in this study, the secondary GPS frequency in DFMC service and L5 PPP service was set to be L2, not L5, to include more usable satellites. However, with the increasing number of the IIF and inclusion of block III satellites in the future, the GPS L1/L5 processing will be used instead (Barrios *et al.*, 2018).

In this study, based on real experiments, the analysis is performed comparing the solution types listed in Table 1. The GNSS signals used for each solution type and the corresponding SBAS augmentation are shown together in Table 1. Note that the solution types discussed in this contributions are in non-aviation mode.

Solution types	GNSS signals	SBAS augmentation
Standalone	GPS L1	No
SBAS L1	GPS L1 + Galileo E1	GPS over L1
SBAS DFMC	GPS L1/L2 + Galileo E1/E5a	GPS + Galileo over L5
PPP over L5	GPS L1/L2 + Galileo E1/E5a	GPS + Galileo over L5

Table 1. Solution types and the GNSS/SBAS signals used in this study

3. PROCESSING STRATEGIES

While SBAS L1 service was discussed in the literature (RTCA, 2016), a few points concerning the new SBAS DFMC is summarized in this section based on EUROCAE (2019). In this mode, using the code and phase observations from the two frequencies, ionosphere-free (IF) code and phase combinations are first formed. Next, IF carrier-smoothed code observations $\tilde{p}_{IF}$ are molded using a Hatch filter with:

$$\tilde{p}_{IF}(t_i) = \frac{1}{N} p_{IF}(t_i) + \frac{N-1}{N} (\tilde{p}_{IF}(t_{i-1}) + \varphi_{IF}(t_i) - \varphi_{IF}(t_{i-1})) \quad (1)$$

where p_{IF} and φ_{IF} represent the IF linear combination of the code and phase measurements in range, respectively. The term N is a pre-defined smoothing window, and t_i and t_{i-1} refer to the current and the previous time epochs. Note that before reaching N the actual number of smoothing epochs n since initialization is used instead in the smoothing process. Based on a

modelled tropospheric delay, the relativistic effects, the SBAS satellite clock corrections and the geometric range modeled using the SBAS satellite orbit corrections and the approximate receiver coordinates, the expectation of the corrected IF code observable $\Delta\tilde{p}_{IF}$ is used to form the observation equation as follows:

$$\mathrm{E}(\Delta\tilde{p}_{IF}) = \underbrace{[G \quad e_G \quad e_E]}_{A} \cdot \underbrace{\begin{bmatrix} \Delta r \\ t_G \\ t_E \end{bmatrix}}_{\Delta x} \tag{2}$$

where the receiver position increments Δr and two separate clock offsets for GPS (t_G) and Galileo (t_E) are estimated. Note that the group delays are to be corrected in $\Delta\tilde{p}_{IF}$ depending on the system and frequencies used. The term $G = [u^1, \cdots, u^m]^T$ contains the satellite-to-receiver unit vectors, with m denoting the number of satellites. The terms e_G and e_E are vectors with elements either equal to zeros or ones, depending on whether the observation is from satellite of the corresponding system, i.e. for GPS satellites the corresponding elements in e_G equal 1, whereas those from Galileo equal zero, and vice versa for e_E. E(.) is the expectation operator. The $\Delta\tilde{p}_{IF}$ is used as input to the SBAS weighted least-squares algorithm, so that the estimated unknown vector $\Delta\hat{x}$, which represents the adjustment to an approximate position and receiver clock offset, can be obtained from

$$\Delta\hat{x} = (A^T Q^{-1} A)^{-1} A^T Q^{-1} \Delta\tilde{p} \tag{3}$$

where Q is the variance-covariance matrix of the corrected IF code observations, which considers the variances of the noise, the multipath, the group delays, the atmospheric residuals and the SBAS corrections in the signal direction.

In the PPP algorithm, the receiver dual-frequency phase observables are processed through a Kalman filter that updates the estimation of the receiver position, the receiver clock offset (one per constellation), the zenith tropospheric delay (ZTD) and each line of sight phase ambiguity. The satellite clock and position information needed for the filter processing is received from the SBAS message.

For ground-based applications under kinematic and complicated measurement environments, users may need to face large multipath interferences and thus much more filter initializations compared to the case in aviation. As defined in EUROCAE (2019), elevation-dependent weighting function is used for smoothed measurements when the number of the smoothing epochs n reaches the smoothing window N. For ground-based applications, e.g., in urban areas, it is however essential to utilize the data with $n < N$ due to the frequent filter initializations and the limited satellite visibility. Making use of the data in urban areas, in Section 4.2, we compare the horizontal positioning results using two different processing strategies. The first strategy excludes the data with the number of the smoothing epochs $n < M$, and applies an elevation-dependent weighting function afterwards. Note that M is here a pre-defined value smaller than the smoothing window N, and is aimed to exclude the data with large residuals at the beginning of smoothing in real time. The second strategy does not exclude any data, but applies a weighting function considering both the elevation angels and the n. Note that $n = N$ when the number of the smoothing epochs reaches N. The variances for the combined IF noise and multipath applying these two strategies, denoted as $\sigma^2_{MP,A}$ and $\sigma^2_{MP.B}$, can be formulated as

$$\sigma^2_{MP,A} = \sigma^2_{0,A} \times \frac{1}{\sin^2(\theta)} \tag{4}$$

$$\sigma^2_{MP.B} = \sigma^2_{0,B} \times \frac{1}{\sin^2(\theta) \times n} \quad (5)$$

where $\sigma^2_{0,A}$ represents the zenith-referenced variance of the *smoothed* IF noise and multipath excluding the data with $n < M$, and $\sigma^2_{0,B}$ represents that of the *raw* IF noise and multipath. $\sigma^2_{0,A}$ and $\sigma^2_{0,B}$ are computed based on the least-squares variance component estimation (LS-VCE) method (Amiri-Simkooei *et al.,* 2009) with the carrier-minus-code terms, making use of the corresponding smoothed and raw IF observations, respectively. The mean values are then removed for each time period with constant ambiguity. The term θ denotes here the elevation angle. The variances of other errors, i.e., the residual atmospheric delays and the SBAS corrections, are computed based on EUROCAE (2019). As in urban areas the filter initializations happen frequently for each satellite at different time points, the number of the smoothing epochs n in (5) mostly differ at the same time point for different satellites.

In the second model (5), the smoothed multipath is assumed to decrease with the increasing n and the increasing elevation angles. It is noted that as the multipath does not behave like the Gaussian white noise, the actual decrease of $\sigma^2_{MP.B}$ with n may not follow Eq. (5), especially in case of large n. It is assumed here that in urban canyons such situation is mostly avoided due to the frequent filter initializations, even when setting a large smoothing window N.

4. EXPERIMENTS AND RESULTS

In this section, experiments performed at the mine sites are described in detail in Section 4.1. The positioning solutions are analysed and compared among different processing strategies with respect to their accuracy and precision. In Section 4.2, data in urban areas are used to test two different weighting models considering and not considering the smoothing time. The data analysis is followed by discussions.

4.1 Experiments at the mine site

In this section, the SBAS tests are performed for mining applications. For experiments at the mine site, the GNSS and the SBAS signals were collected by a Topcon G3-A1 antenna (Topcon, Tokyo, Japan), which is connected with the GMV's magicGNSS User Terminal (magicUT). The receiver can compute SBAS and PPP solutions in ITRF14 in real-time. It can also log the GNSS observation files, navigation files and SBAS messages to compute SBAS L1 and DFMC solutions in magicGEMINI with desired settings. Note that the experiments in this section were performed under harsh weather and work environment in presence of strong sunlight, calx and multipath caused by the mine infrastructure at the mine site. The diagram of the equipment and solutions is given in Figure 2.

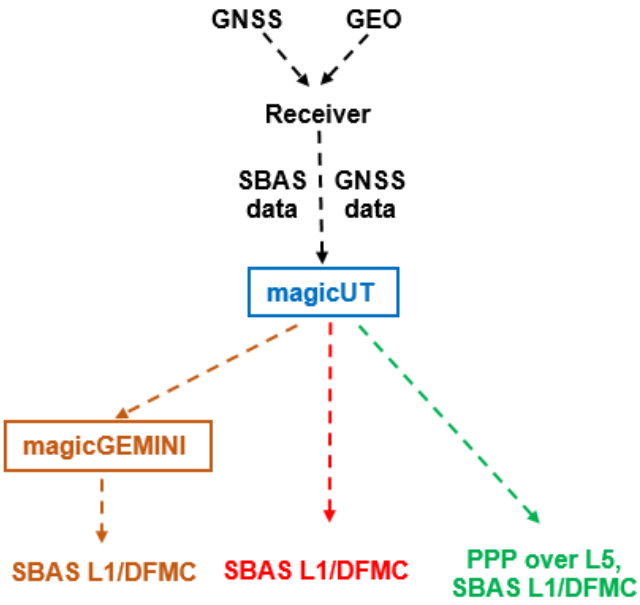

Figure 2. Hardware and software setup used for the mine experiments

The following sections describe the tests and analyse the results obtained. The validation data of each test were obtained via post-processed relative kinematic positioning making use of the data of a reference station nearby. We remark that the SBAS technology can also be used in other applications that require positioning information, such as the establishment of roads, piling, etc. Nevertheless, the performance of SBAS for these applications can also be demonstrated through autonomous experiments on vehicles as will be shown later.

4.1.1 Experiment at mine site: transportation

For real-time positioning, compared to the high-accuracy RTK technology, SBAS is less costly as it does not require a need for maintaining GNSS ground infrastructure around the mine sites. The improved precision and accuracy of SBAS solutions against the traditional standalone solutions can also benefit continuous positioning for autonomous activities, for instance, transportation of ore. The trajectory of the experiment is shown in Figure 3 (Google Earth, 2019).

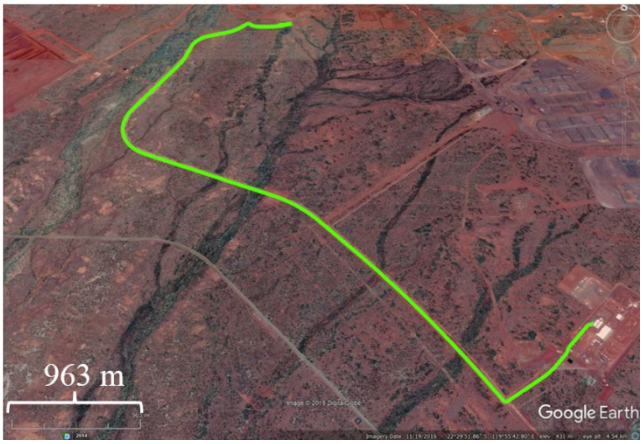

Figure 3. Trajectory of the autonomous car operation in Roy Hill mining site. Image © 2019 DigitalGlobe, © Google Earth (Google Earth 2019)

In this experiment, the kinematic standalone, SBAS L1, DFMC and PPP solutions are compared

using data collected on a car in Roy Hill mining site in Western Australia on August 27, 2018. A Topcon G3-A1 antenna was mounted on top of the car, which was connected to a magicUT receiver (c.f. Figure 2). The positioning errors of the standalone, SBAS and PPP solutions referenced to the validation data are shown in Figure 4. Results confirm that the SBAS L1 (red) and DFMC (green) solutions have better positioning performance than the standalone solutions (blue), currently used. In this study, for the PPP, positioning errors converged to $\pm$0.2 m in the north and east directions and within $\pm$0.3 m in the vertical direction for more than 10 minutes is used as the convergence criterion. Although due to some encountered hardship at the beginning of the test that does not allow enough time for the PPP solution to converge properly, it is still shown to have the best accuracy after around 5 minutes in this experiment. The worst accuracy of the standalone, SBAS L1 and DFMC solutions were during 10 minutes from start, which are related to larger Position Dilution of Precision (PDOP) during this time period, as shown in Figure 5.

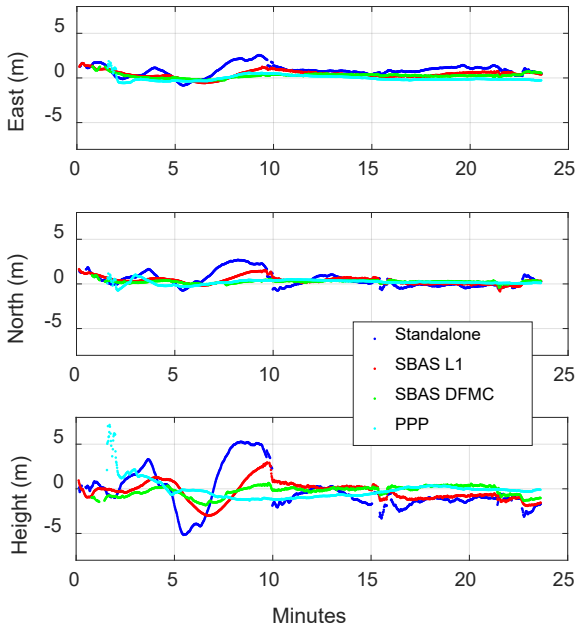

Figure 4. Positioning errors of the standalone, SBAS L1, DFMC and PPP solutions for the autonomous operation test on a vehicle

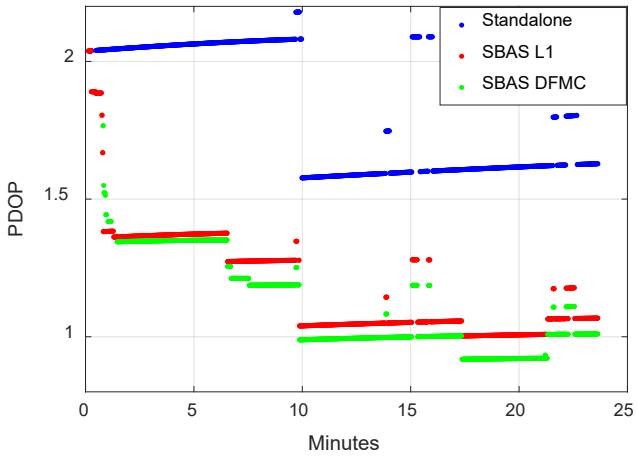

Figure 5. PDOPs of the standalone, SBAS L1 and DFMC solutions for the autonomous operation test on a vehicle

The mean errors, mean absolute errors and standard deviations of the positioning errors of the standalone, SBAS L1, DFMC and PPP solutions are shown in Figure 6. Up to the end of this experiment, the PPP solutions did not fulfill the convergence criterion defined earlier. However, the north/east errors converged to ±0.3 m and the vertical errors converged to ±0.5 m in approximately the last 8 minutes of the experiment. These PPP solutions were used for computing the statistics that are shown in Table 2 along with those for the other modes. From Figure 6 and Table 2 it can be seen that the SBAS solutions generally improve the accuracy and precision when compared to the standalone solutions. Among them, the SBAS DFMC solutions show obvious smaller standard deviations and RMSE compared to the SBAS L1 solutions. Although not very well converged, the PPP solutions have shown the best positioning behaviour. Its standard deviations were at sub-dm level in the east and north directions, and at decimetres in the vertical direction.

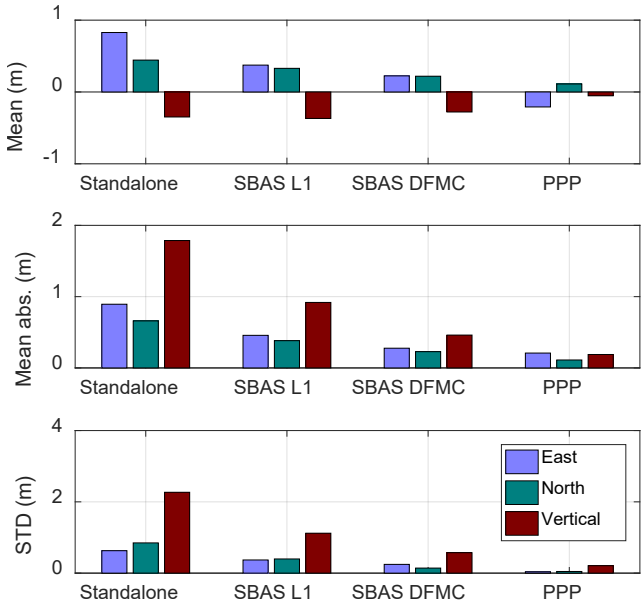

Figure 6. Mean errors, mean absolute errors and standard deviations of the positioning errors of the standalone, SBAS L1, DFMC and PPP solutions

	Metric	Standalone (m)	SBAS and PPP (m)		
			SBAS L1	SBAS DFMC	SBAS-based PPP
East	Mean	0.83	0.37	0.22	-0.21
	Mean abs.	0.89	0.46	0.28	0.21
	STD	**0.63**	**0.37**	**0.25**	**0.04**
	RMSE	1.04	0.53	0.33	0.21
North	Mean	0.44	0.33	0.22	0.11
	Mean abs.	0.66	0.38	0.23	0.11
	STD	**0.85**	**0.40**	**0.14**	**0.05**
	RMSE	0.96	0.52	0.26	0.12
Vertical	Mean	-0.35	-0.37	-0.28	-0.05
	Mean abs.	1.79	0.92	0.46	0.19
	STD	**2.27**	**1.12**	**0.57**	**0.21**
	RMSE	2.29	1.18	0.64	0.22

Table 2. Statistics of the positioning errors in the autonomous operation test on a vehicle

4.1.2 Experiment at mine site: autonomous operation on a drill machine

To test the autonomous operations using SBAS and PPP solutions on a different autonomous machinery, another test was performed at the Roy Hill mine site on November 4, 2018 with the Topcon G3-A1 antenna mounted on a drill machine. Figure 7 shows the drill machine used in the test (left) and the Topcon antenna connected to the magicUT receiver (right). Same as the previous test, the data collected in magicUT was processed with various solution types, i.e. standalone, SBAS L1 and DFMC using magicGEMINI software. The SBAS-based PPP solutions were directly obtained from the magicUT receiver.

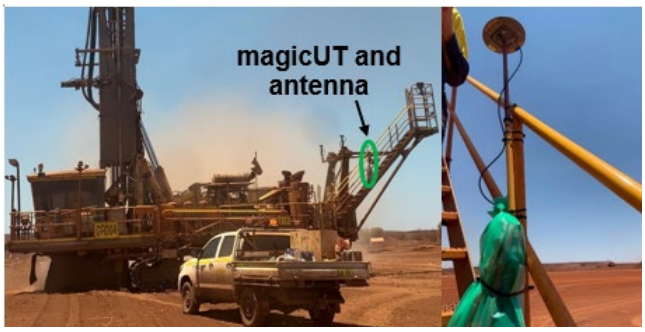

Figure 7. Drill machine used for the autonomous operation (left) and the Topcon antenna mounted on the drill machine zoomed in (right)

The experiment has lasted over one hour so that enough convergence time was available for the PPP solutions. The positioning errors are illustrated in Figure 8 in the east, north and vertical directions for all the solutions. The start of the x-axis represents the first qualified validation data, and the PPP started about 1.4 minutes earlier than the start of the operation. After about 34 minutes after its start, the selected convergence criterion was met, where PPP solutions converged to ±0.2 m in the east and north directions, and to ±0.3 m in the vertical direction for more than 10 minutes. As shown in Figure 8, even before the convergence, the PPP solutions (cyan) have shown the best accuracy among all other types. Moreover, the SBAS DFMC solutions (green) have better positioning performance than the SBAS L1 solutions (red). The systematic effects observed in Figure 8 could be caused by the multipath. Note that the drill machine itself could generate large multipath owing to the signal reflection from its large metallic body.

Once more, the mean errors, mean absolute errors and standard deviations are shown in Figure 9, where PPP solutions after convergence were used for computing the statistics in this mode. The descriptive statistics are given in Table 3. From Figure 9 and Table 3, one can see the positive impact of using SBAS, where improved accuracy and precision can be seen in all SBAS solutions compared to the standalone solutions. Naturally, the PPP solutions were the best, which have shown sub-dm to dm-level precision and accuracy after its convergence. The precision and accuracy of the SBAS L1 and DFMC solutions were at a few decimetres in the east and north directions, and have reached meter-level in the vertical direction.

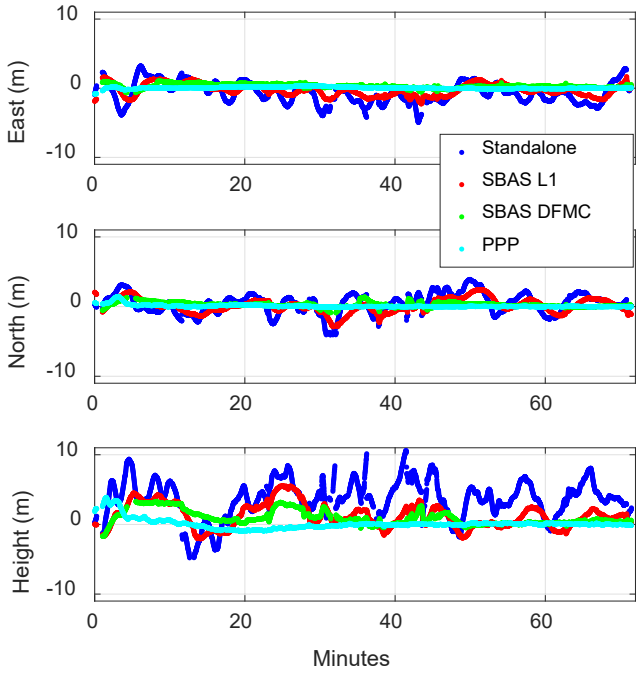

Figure 8. East, north and vertical positioning errors for different solution types for the autonomous operation test on a drill machine

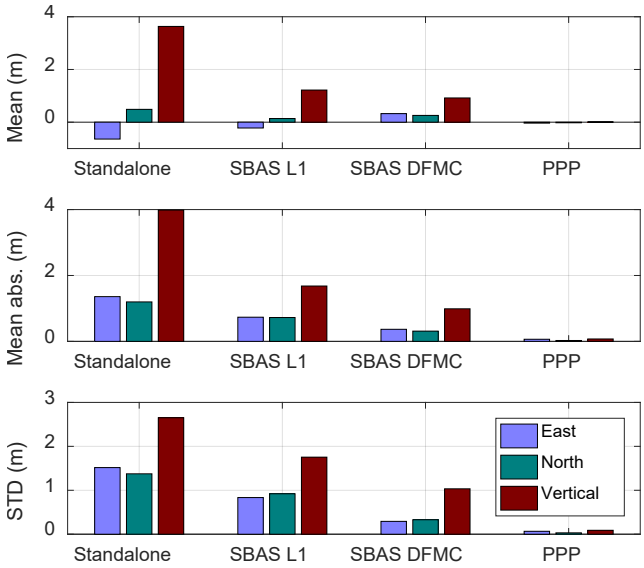

Figure 9. Mean errors, mean absolute errors and standard deviations of the east, north and vertical positioning errors for the autonomous operation test on a drill machine

For autonomous operations on trucks and drill machines, high accuracy and precision at sub-dm to dm level are required in the horizontal directions. As observed in Table 3, only PPP solutions can thus be considered for this application, provided enough convergence time is available.

	Metric	Standalone (m)	SBAS and PPP (m)		
			SBAS L1	SBAS DFMC	SBAS-based PPP
East	Mean	-0.64	-0.22	0.33	-0.04
	Mean abs.	1.36	0.73	0.37	0.06
	STD	**1.52**	**0.83**	**0.29**	**0.07**
	RMSE	1.65	0.86	0.44	0.08
North	Mean	0.49	0.14	0.26	-0.02
	Mean abs.	1.20	0.72	0.31	0.02
	STD	**1.38**	**0.92**	**0.33**	**0.03**
	RMSE	1.46	0.93	0.42	0.04
Vertical	Mean	3.63	1.22	0.92	0.01
	Mean abs.	3.99	1.68	0.99	0.07
	STD	**2.65**	**1.75**	**1.03**	**0.09**
	RMSE	4.50	2.14	1.38	0.09

Table 3. Statistics of the positioning errors in the autonomous operation test on a drill machine

4.2 Experiments in urban areas

The situations under complicated measurement environments, e.g., urban canyons, are different from those at the open-pit mine sites due to the large multipath and the frequent filter initializations when smoothing the code measurements given in (1). In this section, two different weighting models, presented in (4, 5) and denoted as Models A and B, are tested for the SBAS DFMC service using 1 Hz data collected in the urban areas of Sydney for about 20 min on April 19, 2018. The smoothing window N is set to be 4000 epochs. The first strategy applies the elevation-dependent weighting model (4) after excluding the data with the number of the smoothing epochs $n < M$, where M is tested for 0, 10 and 50. The second strategy does not exclude any data, but applies a weighting function related to both the elevation angles and the n. Using data collected during other time periods in the urban areas of Sydney, based on the least-squares variance component estimation (LS-VCE) method (Amiri-Simkooei *et al.*, 2009), the zenith-referenced standard deviation $\sigma_{0,A}$ of the smoothed IF noise and multipath amounts to 0.48 m, 0.43 m and 0.29 m after the data exclusion with M of 0, 10 and 50 epochs, respectively. Exclusion more data at the beginning of the smoothing will help to reduce the amount of data with large residuals during processing, but may also lead to worse satellite geometry and thus degraded precision due to the frequent filter initializations. Testing different M here is aimed to show the different effects of the data exclusion on the positioning results in urban areas. The zenith-referenced standard deviation $\sigma_{0,B}$ of the raw IF noise and multipath amounts to about 0.69 m. The elevation mask is set to 5 degrees.

The RMS of the north and east positioning errors are shown in Table 4 applying $\sigma_{0,A}$ with M of 0, 10 and 50 epochs, and applying $\sigma_{0,B}$. The fourth column lists the RMS of the horizontal errors, where the horizontal errors refer to the square root of the square sum of the north and east errors. The availability here refers to the percentage of the time epochs with the north and the east positioning errors not larger than 10 m and with proper satellite geometry, i.e., with not less than 4 GPS satellites and not less than 5 satellites for GPS and Galileo. From Table 4 it can be observed that applying the Model A, the availability has significantly decreased when increasing the M. This means that in urban areas, increasing the amount of the excluded data at the beginning of smoothing could lead to more time epochs with bad satellite geometry and large outliers. Compared to the Model A with M=0, the Model B delivers similar availability, but smaller horizontal RMSE. Considering the variance convergence in the weighting model is

shown to be important to SBAS DFMC positioning in urban areas, as the data having short smoothing time occupies a large proportion in the total data amount, i.e., about 52% for $n < 50$ in this test. Due to the limited satellite visibility in the urban areas, inclusion of these data in the processing, but appropriately de-weighting them with the smoothing time is helpful to improve the positioning accuracy without degrading the availability.

Model	RMSE North (m)	RMSE East (m)	RMSE Horizontal (m)	Availability
Model A (M=0)	1.377	0.752	1.569	95.1%
Model A (M=10)	1.313	0.760	1.517	80.9%
Model A (M=50)	1.644	0.713	1.792	33.4%
Model B	1.336	0.771	1.542	95.4%

Table 4. RMS of the horizontal positioning errors in urban areas applying Models A and B

5 CONCLUSIONS

This contribution presented the first results of the Australian and New Zealand second-generation SBAS test-bed applied in essential mining operations. In addition to the L1 legacy SBAS signal, the second generation SBAS test-bed provides corrections for GPS and Galileo dual-frequency signals on L1/L2 for GPS and E1/E5a for Galileo, as well as delivering PPP corrections. The planned SBAS system will use L1/L5 measurements of GPS. This configuration offers multiple advantages compared with the traditional SBAS service, in terms of covering a larger area – the Australia-Asia-Pacific region in this case - and providing better performance during fluctuations in the ionosphere. In addition, it enables PPP over the entire coverage area, whereas traditional PPP that acquire the corrections via the Internet is limited to availability of the Internet network.

In this contribution, different types of SBAS modes, including GPS L1 mode and dual-frequency GPS and Galileo (DFMC) solution, in addition to PPP with dual GPS and Galileo observations were assessed with the focus on their usage in mining applications. Experimental kinematic tests were performed at actual mine sites. Results of these methods were analysed and compared. It was found that SBAS solutions generally show better positioning precision and accuracy compared to the standalone solutions, and the SBAS DMFC solutions have shown better positioning precision than the SBAS L1 solutions. For the SBAS DFMC solutions at the mine sites, accuracy at the sub-m level can be obtained in the east and north directions when having enough number of satellites with good geometry. Provided that enough convergence time of tens of minutes is available, the PPP solutions provided the best positioning precision (STD) and accuracy (RMSE) among all solution types. Standard deviations at sub-dm-level can be obtained in the east and north directions and those at sub-decimetres to decimetres can be obtained in the vertical direction. With enough convergence time available, the SBAS-based PPP solutions could reach the accuracy and precision requirements of autonomous operations on trucks and drill machines at mine sites. The results of this study indicate the possibility of SBAS modes to meet high-precision positioning requests for diverse mine applications with reduced cost as only one receiver is used and the Australian SBAS service is free of charge.

Two different weighting models were compared for the SBAS DFMC solutions using the data collected at urban areas with large multipath and frequent filter initializations. It was found that in such environment, considering the smoothing time in the weighting model is helpful to improve the positioning accuracy without degrading the availability of usable positioning solutions.

In the future operational SBAS, when more operational Galileo satellites are available and the GPS constellation is dominated by block IIF and III satellites broadcasting L5 signals, more satellites will be available coupled with improved algorithms and hardware, both at the server and the user end. As such, improvements in positioning performance can be expected compared to the current test-bed results.

ACKNOWLEDGEMENTS

The authors would like to thank FrontierSI, Geoscience Australia (GA), and GMV for their support during this study. Thanks are also given to the Roy Hill team for realizing the experiments at the Roy Hill mine site in Western Australia, and Transport for NSW for the test in Sydney. This study is funded through the project SBAS Test-bed PD8602 – Positional Improvements for Digital Mines, funded by FrontierSI and GA.

REFERENCES

Amiri-Simkooei AR, Teunissen PJG, Tiberius CCJM (2009) Application of least-squares variance component estimation to GPS observables. *Journal of Surveying Engineering* 135(4): 149-160. doi:10.1061/(ASCE)0733-9453(2009)135:4(149).

Barrios J, et al. (2018) Update on Australia and New Zealand DFMC SBAS and PPP System Results. In *Proc. of ION GNSS+* 2018, Institute of Navigation, Miami, Florida, September 24-28, 2018, 1038-1067

Choy S, Kuckartz J, Dempster AG, Rizos C, Higgins M (2017) GNSS satellite-based augmentation systems for Australia. *GPS Solutions* 21(3):835-848. doi: 10.1007/s10291-016-0569-2

Cogdell K, Reddan P (2018) Australia/New Zealand DFMC SBAS and Navigation Message Authentication. In *Proc. of ION GNSS+* 2018, Institute of Navigation, Miami, Florida, September 24-28, 2018, 1068-1083

Dow JM, Neilan RE, Rizos C (2009) The International GNSS Service in a changing landscape of Global Navigation Satellite Systems. *Journal of Geodesy* 83(3-4):191-198. doi: 10.1007/s00190-008-0300-3

EUROCAE (2019) Minimum operational performance standard for Galileo / Global Positioning System/Satellite-Based Augmentation System airborne equipment. The European Organisation for Civil Aviation Equipment. ED-259. February 2019

El-Mowafy A (2015) Estimation of Multi-Constellation GNSS Observation Stochastic Properties Using a Single-Receiver Single-Satellite Data Validation Method. *Survey Review*, 47(341): 99-108. doi:10.1179/1752270614Y.0000000100

El-Mowafy A, Deo M, Kubo N (2017) Maintaining real-time precise point positioning during outages of orbit and clock corrections. *GPS Solutions* 21(3): 937-947. doi: 10.1007/s10291-016-0583-4

Google Earth (2019) Google Earth imagery on November 19, 2016. Google Earth 7.3.2.5495, Roy Hill, Australia, 22° 29’ 51.86”S, 119° 55’ 42.80”E, Eye alt 4.54 km. Image © 2019 DigitalGlobe. https://www.google.com/earth/ (March 7, 2019)

ICSM (2018) Geocentric Datum of Australia 2020 Technical Manual, Version 1.2. ICSM, PCG, August 24, 2018

MOPS (2017) Minimum Operational Performance Specification for Galileo/Global Positioning System/Satellite-Based Augmentation System Airborne Equipment. SBAS DFMC L5 MOPS Draft WG62_GAL_GPS_SBAS_MOPS_v0.3.8_10_Mar_2017

Noll C, Bock Y, Habrich H, Moore A (2009) Development of data infrastructure to support scientific analysis for the International GNSS Service. *Journal of Geodesy* 83(3-4):309-325. doi:

10.1007/s00190-008-0245-6

RTCA (2016) RTCA DO-229E, Minimum Operational Performance Standards for Global Positioning System/Satellite-Based Augmentation System Airborne Equipment, 2016.

Sarab T, Marais J (2013) Weighting models for GPS Pseudorange observations for land transportation in urban canyons. *The 6th European Workshop on GNSS Signals and Signal Processing*, December 2013, Germany, 4p, hal-00942180

Sobreira H, Bougard B, Barrios J, Calle JD (2018) SBAS Australian-NZ Test Bed: Exploring New Services. In *Proc. of ION GNSS+* 2018, Institute of Navigation, Miami, Florida, September 24-28, 2018, 2119-2133

Suard N, Gurtner W, Estey L (2003) Proposal for a new RINEX-type Exchange File for GEO SBAS Broadcast Data. Available at ftp://igs.org/pub/data/format/geo_sbas.txt.

Technical Specifications (2017) Technical Specifications Document for Satellite-Based Augmentation System (SBAS) Testbed. Revision 5, November 10, 2017